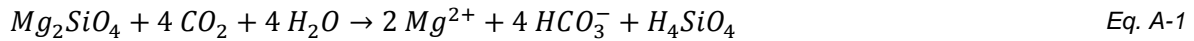


Supplementary Material

A. Weathering efficiency of used rock material	2
B. Empirical relationship between SSA and grain size.....	3
C. Empirical relationship between energy demand and grain size	5
D. Energy demand in dependence of feed grain size.....	6
E. The optimal grain size	7
F. Temperature influence on weathering – regional factors	8
G. Grain surface area based weathering rates.....	9
H. Identification of suitable land for Enhanced Weathering	11
I. Identification of global regions for the model	13
J. Economic assessment of rock mining and production	15
K. Distance to source distribution, case Indonesia.....	19
L. Distribution of source rocks	20
M. Regional supply curves	21
N. References.....	25

A. Weathering efficiency of used rock material

The theoretical weathering efficiency calculation is based on the dissolution of pure forsterite, following the stoichiometric equation:



This is the theoretical upper limit of CO₂ fixation, which is not achieved in nature, since the forsterite is deposited together with various minerals during genesis. Thus, impurities and general heterogeneity in the source material, as well as equilibration effects with the atmosphere after dissolution (1) decrease the overall potential.

The upper limit for our study was derived from Moosdorf, Renforth and Hartmann (2), who give a range for ultramafic rocks, which would best represent the occurrence of forsterite material in nature.

An estimate for the average efficiency of basalt was calculated after Renforth (3) using average basalt geochemical data of the GEOROC database (4) for % CaO and % MgO:

$$\Pi = \frac{M_{CO_2}}{100} \left(\frac{\% CaO}{M_{CaO}} + \frac{\% MgO}{M_{MgO}} \right) \cdot \omega \quad \text{Eq. A-2}$$

with M_x being the molar masses of the attributed oxides and ω as a factor of additional drawdown from cation flux into the ocean (cf. (3) and references therein).

Tab. A-1

material	Weathering efficiency Π (t CO ₂ t rock ⁻¹)	source
forsterite	1.25	stoichiometric calculation
ultramafic rocks	0.8 – 1.1	Moosdorf, Renforth and Hartmann (2)
basalt	0.3 ± 0.1	calculated from geochemical data by Sarbas (4)

B. Empirical relationship between SSA and grain size

Since most studies on energy demand report either grain sizes or specific surface area, a relationship was developed: Some studies published the relationship between grain size and specific surface area based on empirical values from lab ground minerals of quartz, albite and dunite, but those consider only grain sizes > 40 μm (5-7). Moosdorf, Renforth and Hartmann (2) published simulation data in their supplement, which considers the range of about 1-10 μm. If these data are combined with the data from above for dunite, the following empirical relationship is achieved:

$$SSA (m^2 g^{-1}) = 69.18 * grain\ size [\mu m]^{-1.24} \quad Eq. B-1$$

To compare reported values from the literature with an idealised model, the specific surface area was calculated for 1 g of perfectly sphere-shaped dunite grains, with a diameter corresponding to the grain size. Fig. B1 shows a significant difference in the relationship between grain size and specific surface area if idealised sphere based models are considered. Depending on the grain size, the calculated surface area is up to 40 times higher for the observation than the ideal assumption. This is not unusual considering the irregularity of natural grains and the different forms of meso- and macropores. However, this shows that the shrinking core model used in some studies (8, 9) does strongly underestimate the SSA.

Tab. B-1: Fit parameters for the relationship between grain size and specific surface area

Fit type: linear model, $f(x) = p1 \times x + p2$ (based on logarithmised values)

parameter	p1	p2	goodness of fit	
fit	-1.242	1.84	SSE	5.1926
upper 95% bound	-1.476	1.432	r ²	0.8139
lower 5% bound	-1.007	2.248	RMSE	0.4385

Converted to a power function: $SSA = a \times GS^b$ (based on linear model results)

parameter	a	b
fit	69.183	-1.242
upper 95% bound	27.0396	-1.476
lower 5% bound	177.0109	-1.007

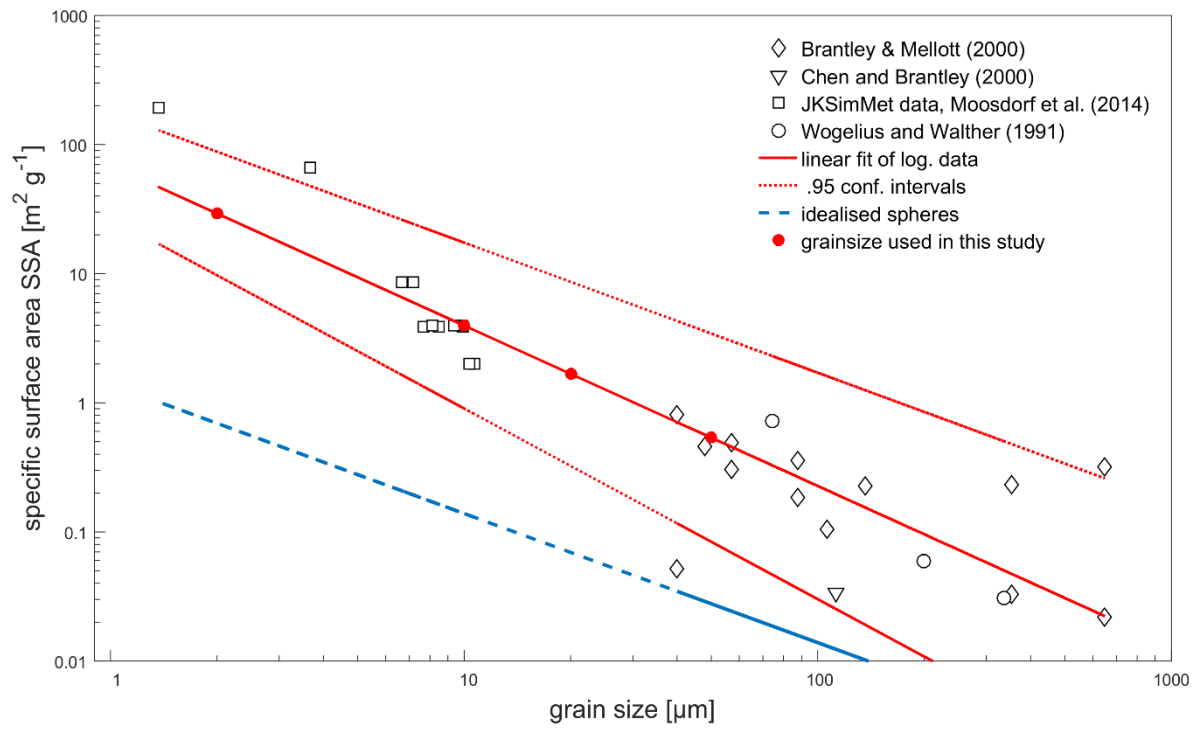


Fig. B-1: Relationship between grain size and specific surface area

C. Empirical relationship between energy demand and grain size

Since in our study, the grain size is the first order determinant of the weathering efficiency, a relationship between energy input for comminution and the corresponding grain size product is needed to evaluate energy demand related to weathering efficiency. Considered data refers to the p_{80} value, which is the grain size at which only 20% are held back in the sieve, meaning that 80% of the material are of the given grain size or smaller.

Tab. C-1: Fit parameters for the relationship between energy demand and specific surface area

Fit type: linear model, $f(x) = p1 \times x + p2$ (based on logarithmised values)

parameter	p1	p2	goodness of fit	
fit	-1.162	0.821	SSE	7.1430
upper 95% bound	-1.322	0.557	r^2	0.8191
lower 5% bound	-1.002	1.086	RMSE	0.3898

Converted to a power function: $ED = a \times GS^b$ (based on linear model results)

parameter	a	b
fit	6.62	-1.162
upper 95% bound	3.61	-1.322
lower 5% bound	12.19	-1.002

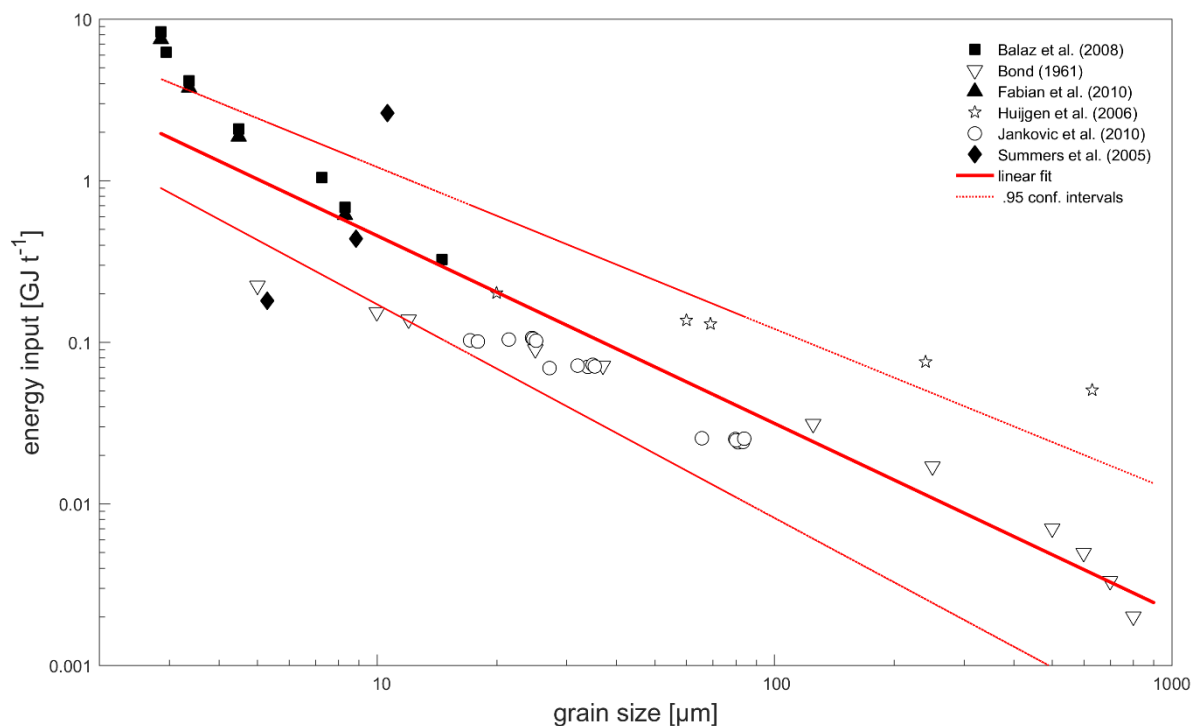


Fig. C-1: Relationship between comminution output grain size and energy demand. Considered data is taken from Jankovic, Dundar and Mehta (10), calculation after the Bond law (11), Baláž, et al. (12), Fabian, et al. (13), Summers, Dahlin, Rush, O'Connor and Gerdemann (14), and Huijgen, Ruijg, Comans and Witkamp (15). Data indicated by filled symbols were given as SSA and recalculated to grain size via an empirical function (Eq. B-1, App. B).

D. Energy demand in dependence of feed grain size

The energy demand for rock comminution depends on the ratio between feed input (F_{80} , where 80% of the material is of the given grain size or smaller) and targeted (P_{80}) grain size of the applied rock material. According to the Bond law (11), the differences in feed grain size become significant only for the smallest grain sizes, so that differences in the feed grain size (varying in the cited data between 40 μm and >3 mm) are within the general uncertainty of the data fit.

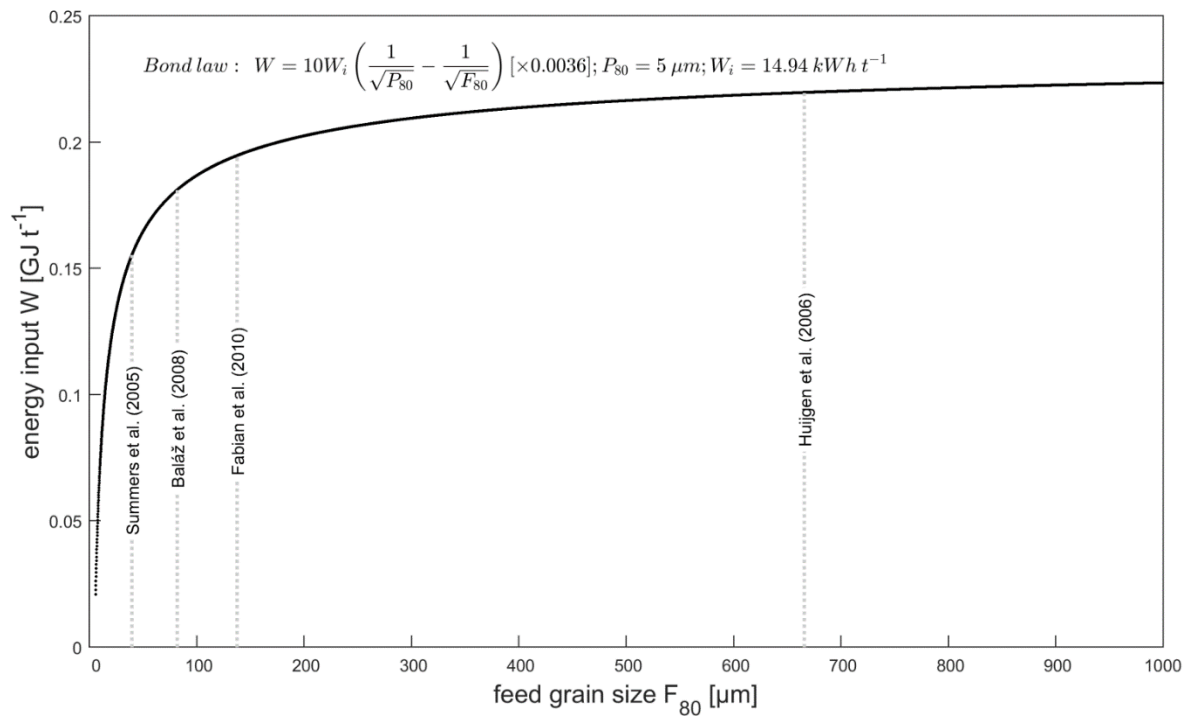


Fig. D-1: The development of necessary energy input considering varying feed grain sizes at fixed product grain (P_{80}) size of 5 μm and work index $W_i = 14.94 \text{ kWh t}^{-1}$. Vertical lines indicate the feed grain sizes reported in the references, the considered grain size/energy input data was taken from.

E. The optimal grain size

Costs, revenues, and profits depend mainly on the deployed grain size. On the one hand, the grinding energy demand increases with decreasing target grain sizes, pushing up costs. At the same time, the speed of weathering increases due to increased surface area, thus increasing the carbon dioxide removal potential per area. We assume that each ton of CO₂ removed from the atmosphere is rewarded at a certain price, which could be either a payment per ton of CO₂ at the level of a given carbon tax or the issuance of a newly created emission permit that can be sold at a certain price on the carbon market. It is also assumed that the carbon price increases at 5% per year.

The revenues R per area are equal to the amount of carbon removed in a given year times the carbon price τ_{CO_2} in that year. Assuming that the field was fully loaded with rock powder in this year, the revenue is given by

$$R(x) = M \delta(x) \Pi \tau_{CO_2}. \quad \text{Eq. E-1}$$

For the steady state, the costs $C(x)$ can be calculated as the costs per ton rock times the rock mass per area, $M \delta(x)$, that need to be applied to replenish the field. As described above, the costs per ton rock consist of fixed costs for investment, O&M, and transport and distribution C_{fix} and of electricity costs for grinding that depend on the grain size $C_e(x)$,

$$C(x) = M \delta(x) [C_{fix} + C_e(x)]. \quad \text{Eq. E-2}$$

Fig. D-1a shows total global costs, revenues and profits as a function of grain size. For the profits $P(x) = R(x) - C(x)$ to be positive, the carbon price has to exceed the threshold $\tau_{CO_2} > [C_{fix} + C_e(x)] / \Pi$. This implies that larger grainsizes which have lower electricity costs C_e are profitable at a lower carbon price. Using the functional forms $C_e(x) = c_1 x^{c_2}$ (see SI C) and $\delta(x) = d_1 x^{d_2}$ (see Eq. 2 and SI B), we can calculate the optimal grain size X_{opt}

$$X_{opt} = [(d_2 (\Pi \tau_{CO_2} - C_{fix}) / (c_1 (c_2 + d_2)))]^{1/c_2}. \quad \text{Eq. E-3}$$

This relation is shown in Fig. E-1b for basalt, showing that the optimal grain size drops very quickly once the carbon price is high enough for Enhanced Weathering to become competitive.

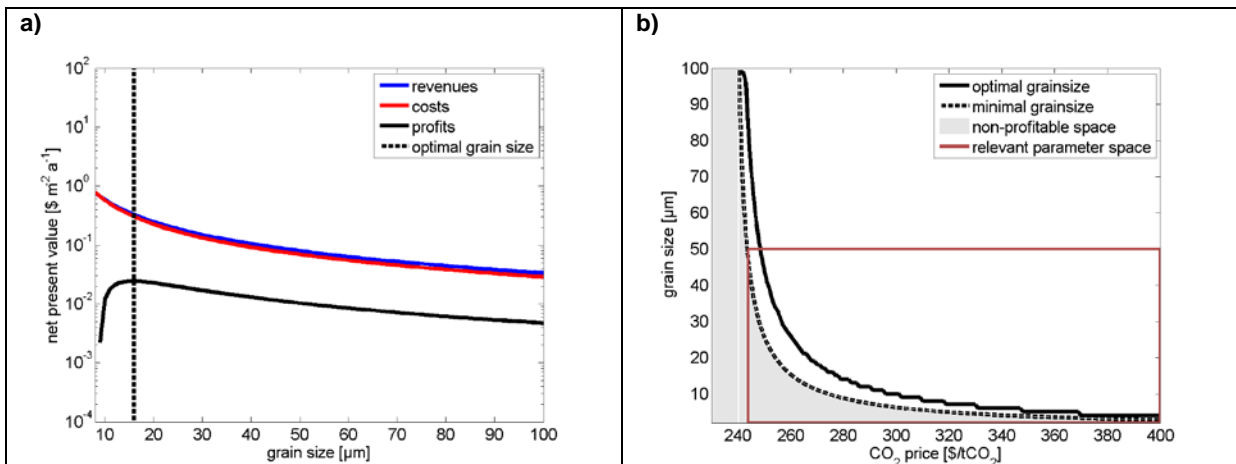


Fig. E-1: (a) Costs (red), revenues (blue) and profits (black) for basalt per square meter land as a function of grain size ($\tau_{CO_2} = 280$ \$/tCO₂). At an optimal grain size of 16 μm, profits are maximized. (b) Optimal grain size of basalt as a function of carbon price. The dashed line shows the minimal grainsize that is still profitable for a given carbon price. Parameter values: Electricity price 23.8\$/GJ, $\Pi = 0.3$, fixed costs 77.0\$/t rock (see Tab. J-5, assuming a transport distance of 300km), electricity demand for grinding as in SI C, carbon removal rate as in Tab. 1.

F. Temperature influence on weathering – regional factors

The carbon removal rates strongly depend on chemical weathering rates, which are significantly driven by temperature. For the given differentiation (temperate and tropical) the following assumptions are made for weathering rates in dependence of the ambient temperature. Factors were calculated, which are based on the standard temperature of 25°C. Annual mean temperatures were calculated for each climate class. The factor is determined by the Arrhenius reaction speed dependency on temperature:

$$k = Ae^{\frac{-E_A}{RT}} \quad \text{Eq. F-1}$$

With k = rate constant, A = pre-exponential factor (omitted here), E_A =activation energy (here 50 000 J/mol after Hartmann, Moosdorf, Lauerwald, Hinderer and West (16)), R = universal gas constant and T = absolute temperature.

Data for annual mean temperature were taken from the WorldClim data (17; resolution: 1 km²).

Tab. F-1 Regionalised weathering rate factors to account for annual average temperatures.

	warm	temperate
annual mean temperature (°C)	24.3 ± 2.95	10.2 ± 4.15
factor (relative to 25°C)	0.95 ± 0.20	0.35 ± 0.22

G. Grain surface area based weathering rates

The considered weathering rate estimates are based on generalized equations for forsterite published by Bandstra and Brantley (18). Assuming a dunite rock containing only forsterite and under standard conditions of 25°C, pH dependent rates are calculated using

$$R_{dunite}[\text{mol m}^{-2}\text{s}^{-1}] = k_{H^+} \cdot 10^{n_{H^+} \cdot \text{pH}} \quad \text{Eq. G-1}$$

For dunite, with $k_{H^+} = 5.55 \times 10^{-8} \pm 6.63 \times 10^{-9} \text{ mol m}^{-2}\text{s}^{-1}$ and $n_{H^+} = 0.372 \pm 0.0053$, and

$$R_{basalt}[\text{mol m}^{-2}\text{s}^{-1}] = (\hat{k}_{H^+} \cdot 10^{-n_{H^+} \cdot \text{pH}} + \hat{k}_{OH^-} \cdot 10^{n_{OH^-} \cdot (\text{pH}-14)}) \cdot e^{\left(\frac{-E_a}{R \cdot T}\right)} \quad \text{Eq. G-2}$$

for basalt, with $\hat{k}_{H^+} = 588 \pm 558 \text{ mol m}^{-2}\text{s}^{-1}$, $n_{H^+} = 1.16 \pm 0.107$, $\hat{k}_{OH^-} = 0.0822 \pm 0.079 \text{ mol m}^{-2}\text{s}^{-1}$, $n_{OH^-} = 0.16 \pm 0.0309$, $E_a = 47500 \pm 2690 \text{ J mol}^{-1}$, $T = 298\text{K}$, and $R = 8.314472 \text{ J mol}^{-1}\text{K}^{-1}$.

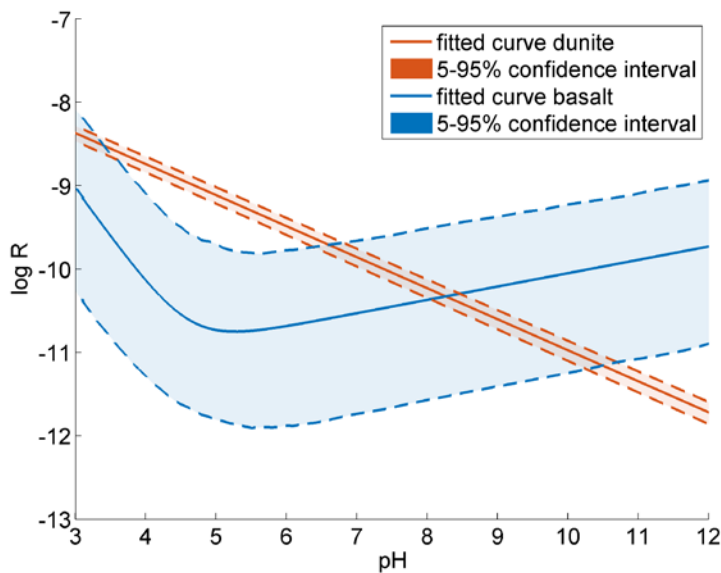


Fig. G-1: Fitted curves for logarithmised weathering rates based on Eqs. G-1 and G-2. The uncertainty was calculated numerically using a Monte-Carlo Simulation, assuming log-normal distributed parameters.

Tab. G-1 Overview over pH dependent weathering rate variability, calculated after equations based on literature value compilations (18) $T=25^\circ\text{C}$, uncertainty range in brackets, and carbon sequestration potential Π .

pH	rate ^a [$\log \text{ mol m}^{-2} \text{ s}^{-1}$] at given pH			Renforth et al. (16)	Carbon sequestration potential Π
	4	7	9		
basalt	-10.13 (-8.96 – -12.33)	-10.53 (-9.55 – -12.63)	-10.21 (-9.22 – -12.25)		0.3
dunite	-8.74 (-8.67 – -8.82)	-9.86 (-9.77 – -9.95)	-10.60 (-10.51 – -10.71)	-11.8	1.1

^a rates for basalt are reported as mol Si; according to (14): 1 mol Si per mol basalt: $\text{Ca}_{0.3}\text{Mg}_{0.1}\text{Fe}_{0.4}\text{Al}_{0.3}\text{SiO}_{3.25}$

Tab. G-2: Average (upper/lower bound in brackets) relative amount of spread material (dunite, basalt) dissolved within one year for different grain sizes at a pH of 7.

Grain size	Dunite	Basalt
	(fraction dissolved per year)	
50 μm	0.33 (0.27 – 0.41)	0.07 (0.001 – 0.6)
20 μm	1.03 (0.84 – 1.27)	0.22 (0.002 – 1.87)
10 μm	2.44 (1.98 – 3.00)	0.52 (0.004 – 4.43)
2 μm	17.95 (14.59 – 22.08)	3.84 (0.023 – 3.26)

H. Identification of suitable land for Enhanced Weathering

Classification is done by land use and climate zone (as proxy for temperature and runoff). The classification was based on data, compiled in the global ecophysiology map by Sayre, *et al.* (19). The following classes were distinguished, to derive two grades:

Grade 1

- a) Rainfed and irrigated croplands in hot and wet climate
- b) Predominantly cropland in hot and wet climate

Grade 2

- c) Rainfed and irrigated croplands in temperate climate
- d) Predominantly cropland in temperate climate

Not considered:

- e) Not suitable because: too cold, too dry, no or minor cropland area

Land use

We assume that the most suitable land would be cropland that is actively used. Using any agricultural land would include pastures and grassland, which are assumed to be less suitable for the rock powder application because the soils are not regularly reworked.

To identify the suitable land areas, the satellite dataset GlobCover (20) provided by ESA and included in the ecophysiology map was used. Two categories were distinguished (Tab. H-1).

Tab. H-1 Selected land cover classes from the ecophysiology map.

purely cropland	predominantly cropland
<i>GLC_val class</i>	<i>GLC_val class</i>
11 Post-flooding or irrigated croplands (or aquatic)	20 Mosaic cropland (50-70%) / vegetation (grassland/shrubland/forest) (20-50%)
14 Rainfed croplands	

Bioclimate

Weathering rates are strongly dependent on temperature and water availability. To approach these parameters on a global scale, the bio climate classification was used, selecting the classes given in Tab. H-2.

Tab. H-2 Selected bio climate classes from the ecophysiology map.

warm and moist	temperate
<i>Bio_val class</i>	<i>Bio_val class</i>
23 hot, wet	10 cool, very wet
24 hot, moist	11 cool, wet
28 hot, very wet	14 warm, wet
33 very hot, wet	15 warm, very wet
34 very hot, moist	
36 very hot, very wet	

The bioclimate classification is based on temperature (GDD, growing degree days, Eq. H-1) and aridity (AI, aridity index, Eq. H-2).

$$GDD = \sum_{n=1}^{12} T_{mean(n)} \times days(n) \quad \text{Eq. H-1}$$

$$AI = \frac{precipitation}{evapotranspiration} \quad \text{Eq. H-2}$$

Resulting in the final classification given in Tab. G-3 and used for the classes selected in Tab. H-2.

Tab. H-3 Differentiation of bioclimate classes after temperature and aridity.

GDD	class	AI	class
9000-13500	very hot	1.5-70	very wet
7000-9000	hot	1.0-1.5	wet
4500-7000	warm	0.6-1.0	moist
2500-4500	cool		

I. Identification of global regions for the model

Regional definition is based on Leimbach et al. (2015) with the following modifications:

1. Taiwan and China merged into one region
2. Regions separated into high, middle and low income groups were merged (EU12-H and EU12-M, LAM-M and LAM-L, MEA-H and MEA-M, OAS-M and OAS-L, SSA-M and SSA-L).

Tab. I-1: Regional definitions

Single-country regions	Countries
BRA	Brazil
CAN	Canada
IDN	Indonesia
IND	India
JPN	Japan
KOR	Republic of Korea
MEX	Mexico
RUS	Russian Federation
SAF	South Africa
TUR	Turkey
Aggregated regions	Countries
AUNZ	Australia; New Zealand
CAS	Armenia; Azerbaijan; Georgia; Kazakhstan; Kyrgyz Republic; Tajikistan; Turkmenistan; Uzbekistan
CHN	China; Hong Kong, SAR; Macao, SAR; Taiwan
EEU	Albania; Bosnia and Herzegovina; Croatia; Macedonia FYR; Montenegro; Serbia
EEU-FSU	Belarus; Moldova; Ukraine
EFTA	Iceland; Norway; Switzerland
EU12	Bulgaria; Cyprus; Czech Republic; Estonia; Hungary; Latvia; Lithuania; Malta; Poland; Romania; Slovak Republic; Slovenia
EU15	Austria; Belgium; Denmark; Finland; France; Germany; Greece; Ireland; Italy; Luxembourg; Netherlands; Portugal; Spain; Sweden; United Kingdom
LAM	Antigua and Barbuda; Argentina; Bahamas, The; Barbados; Belize; Bermuda; Bolivia; Chile; Colombia; Costa Rica; Cuba; Dominica; Dominican Republic; Ecuador; El Salvador; French Guiana; Grenada; Guadeloupe; Guatemala; Guyana; Haiti; Honduras; Jamaica; Martinique; Netherlands Antilles; Nicaragua; Paraguay; Panama; Peru; St. Lucia; St. Kitts and Nevis; St. Vincent and the Grenadines; Suriname; Trinidad and Tobago; Uruguay; Venezuela, RB;
MEA	Bahrain; Iran, Islamic Rep.; Iraq; Israel; Jordan; Kuwait; Lebanon; Occupied Palestinian Territory; Oman; Qatar; Saudi Arabia; Syrian Arab Republic; United Arab Emirates; Yemen, Rep.
NAF	Algeria; Egypt, Arab Rep.; Libya; Morocco; Tunisia; Western Sahara
OAS	Bangladesh; Bhutan; Brunei Darussalam; Fiji; French Polynesia; Guam; Korea, Dem. Rep.; Nepal; New Caledonia; Malaysia; Maldives; Micronesia, Fed. Sts.; Myanmar; Papua New Guinea; Philippines; Samoa; Singapore; Solomon Islands; Sri Lanka; Thailand; Timor-Leste; Tonga; Vanuatu; Cambodia; Lao PDR; Mongolia; Vietnam
PAK	Afghanistan; Pakistan
SSA	Angola; Benin; Botswana; Burkina Faso; Burundi; Cameroon; Cape Verde; Central African Republic; Chad; Comoros; Congo, Dem. Rep.; Congo, Rep.; Cote d'Ivoire; Djibouti; Eritrea; Ethiopia; Equatorial Guinea; Gabon; Gambia, The; Ghana; Guinea; Guinea-Bissau; Kenya; Lesotho; Liberia; Madagascar; Malawi; Mali; Mauritania; Mauritius; Mozambique; Namibia; Niger; Nigeria; Rwanda; Sao Tome and Principe; Senegal; Sierra Leone; Somalia; Sudan; Swaziland; Tanzania; Togo; Uganda; Zambia; Zimbabwe
USA	United States; Puerto Rico; United States Virgin Islands

Tab. I-2: Cropland (in 10⁶ km²) available for rock application, given for the two general climate regimes defined in SI G.

Region	warm	temperate	total
AUNZ	0.002	0.133	0.135
BRA	1.101	0.034	1.135
CAN	0	0.004	0.004
CAS	0	0.013	0.013
CHN	0.397	0.649	1.046
EEU	0	0.032	0.032
EEU-FSU	0	0.265	0.265
EFTA	0	0.002	0.002
EU12	0	0.222	0.222
EU15	0.004	0.464	0.467
IDN	0.542	0.004	0.546
IND	1.190	0.011	1.201
JPN	0.003	0.079	0.082
KOR	0	0.002	0.002
LAM	0.354	0.142	0.496
MEA	0.004	0.009	0.013
MEX	0.022	0.000	0.023
NAF	0.007	0.006	0.013
OAS	1.101	0.018	1.120
PAK	0.012	0.008	0.020
RUS	0	0.454	0.454
SAF	0.002	0.001	0.003
SSA	0.354	0.039	0.393
TUR	0.007	0.028	0.035
USA	0.025	0.154	0.180
TOTAL	5.128	2.774	7.903

J. Economic assessment of rock mining and production

Investment costs and operation and maintenance costs for the mining and grinding of suitable source rocks are estimated from selected preliminary economic assessment reports of open pit mines (after Canadian National Instrument 43-101). Here, only data for the processed material (in most cases metal ores) was used. Given data in the main text is derived from the following data, extracted from the written reports, available as PDF online.

Tab. J-1 Extracted data for investment costs from selected preliminary economic assessment reports of open-pit mines (as listed in Curry, Ismay and Jameson (21)).

	report currency and conversion (if given in the report)	mining	ore processing	waste rock handling	Infra- structure	other	Investment TOTAL
(original currency / converted to USD (average of 2014))							
Authier	1 USD = 1 CAD 2012	0.02 / 0.02	2.48 / 2.57	1.07 / 1.11	0.68 / 0.7	0.58 / 0.6	4.83 / 5
Lac a Paul	1 CAD=0.9524 USD 2013	2.85 / 2.85	18.8 / 18.81	1.49 / 1.49	0.43 / 0.43	13.51 / 13.52	37.07 / 37.1
Toroparu Gold	USD Q4 2012	0.12 / 0.12	0.59 / 0.6	0 / 0	0.05 / 0.05	0.66 / 0.67	1.41 / 1.45
Hasbrouck Property	USD 2011	0.18 / 0.17	0.53 / 0.51				0.71 / 0.68
Tasiast Mine	USD 2011					0.25 / 0.24	0.25 / 0.24
Pirquitas Mine	USD 2011	12.66 / 12.09	20.21 / 19.3	1.72 / 1.64	7.33 / 7	3.06 / 2.92	44.98 / 42.95
Kitsault	CAD (1 CAD = 0.92 USD) 2010	0.24 / 0.22	1.03 / 0.95	0.55 / 0.51	0.21 / 0.19	0.93 / 0.86	2.95 / 2.72
Mount Hope	USD 2007	0.06 / 0.06	0.51 / 0.5	0 / 0	0.01 / 0.01	0.07 / 0.07	0.65 / 0.63
Deer Horn	CAD 2013	0.26 / 0.25	15.81 / 15.36	0 / 0	0.26 / 0.25	1.15 / 1.11	17.47 / 16.98
El Morro	USD 2011						
Kwanika	CAD (1 CAD = 0.95 USD (Q4 2012))	0.28 / 0.27	2.85 / 2.75	0.2 / 0.19	0.32 / 0.31	0.39 / 0.38	4.05 / 3.9
Hycroft Mine	USD (Q2 2011)	0.12 / 0.11	1.38 / 1.28	0.06 / 0.05	0.02 / 0.01	0.03 / 0.03	1.6 / 1.48
Springpole Gold	USD (Q1 2013)	0.64 / 0.64	0.31 / 0.31	0.64 / 0.64	0.61 / 0.61	0.55 / 0.55	2.73 / 2.75
Taca Taca	USD (2012)	0.5 / 0.52	1.51 / 1.57	0.78 / 0.81	0.19 / 0.19	0.83 / 0.86	3.81 / 3.94

Tab. J-2 Extracted data for operation and maintenance costs from selected preliminary economic assessment reports of open-pit mines (as listed in Curry, Ismay and Jameson (21)).

	report currency and conversion (if given in the report)	mining	grinding	general & administration	O&M TOTAL
(original currency / converted to USD (average of 2014))					
Authier	1 USD = 1 CAD 2012	10.02 / 10.37	13.83 / 14.31	5.02 / 5.19	28.87 / 29.86
Lac a Paul	1 CAD=0.9524 USD 2013	27.3 / 27.32	48.1 / 48.14	4.3 / 4.3	79.7 / 79.76
Toroparu Gold	USD Q4 2012	13.82 / 14.16	10.51 / 10.77	6.76 / 6.93	31.09 / 31.87
Hasbrouck Property	USD 2011	1.41 / 1.35	2.68 / 2.56	0.37 / 0.35	4.46 / 4.26
Tasiast Mine	USD 2011	18.14 / 17.32		9.51 / 9.08	27.65 / 26.4
Pirquitas Mine	USD 2011	9.63 / 9.19	17.05 / 16.28	7.74 / 7.39	34.42 / 32.86
Kitsault	CAD (1 CAD = 0.92 USD) 2010	2.47 / 2.28	4.74 / 4.37	1.09 / 1.01	8.3 / 7.65
Mount Hope	USD 2007	3.19 / 3.09	3.62 / 3.51		6.81 / 6.6
Deer Horn	CAD 2013	32.4 / 31.48	23 / 22.35	5.7 / 5.54	61.1 / 59.36
El Morro	USD 2011	5.52 / 5.27	7.14 / 6.82	2.65 / 2.53	15.31 / 14.62
Kwanika	CAD (1 CAD = 0.95 USD (Q4 2012))	2.6 / 2.5	10.69 / 10.3	1.2 / 1.16	14.49 / 13.96
Hycroft Mine	USD (Q2 2011)	1.03 / 0.95	6.79 / 6.27	0.37 / 0.34	8.19 / 7.56
Springpole Gold	USD (Q1 2013)	2.78 / 2.8	10.56 / 10.62	0.87 / 0.87	14.2 / 14.29
Taca Taca	USD (2012)	4.69 / 4.85	4.26 / 4.41	0.82 / 0.85	9.77 / 10.11

Tab. J-3: Basic statistics on data. All data are converted from currency in the report to US \$/t (normalised to US \$ rate: 2014 average). Detailed compilation of data including references can be found in Tab. J-1 and Tab. J-2. *Data from Daniel, Lane and McLean (22) show an average share of 44±7% (n=6) of energy costs over the total operation costs for different locations and grinding technologies (see Tab. I-4 for details). Targeted grain sizes will be smaller than the average in the study data (range 2 – 100 µm), while hardness will be higher, so that costs may represent a lower estimate. We therefore use the 75-percentile costs as best estimate. Median and maximum are taken as lower and upper bounds, respectively.

	mean	n	stdev	median	range	p25	p75
product grain size (µm)	91.15	13	60.97	75.00	24 - 200	44.00	150.00
material hardness (Bond work index, kwh/t)	14.94	10	2.50	14.50	11.8 - 18.5	12.80	16.98
investment costs [US \$/t]							
mining	1.44	12	3.44	0.24	0.02 - 12.09	0.12	0.55
ore processing	5.37	12	7.60	1.42	0.31 - 19.3	0.58	5.90
waste rock handling	0.81	8	0.58	0.72	0.05 - 1.64	0.43	1.20
infrastructure	0.89	11	2.04	0.25	0.01 - 7	0.12	0.52
other	1.82	12	3.76	0.64	0.03 - 13.52	0.34	0.92
investment TOTAL	9.22	13	14.38	2.75	0.03 - 13.52	1.45	5.00
O&M costs [US \$/t]							
mining	9.50	14	9.81	5.06	0.95 - 31.48	2.58	13.21
grinding	12.36	13	12.17	10.30	2.56 - 48.14	4.41	14.31
general & administration	3.50	13	3.06	2.53	0.34 - 9.08	0.87	5.54
O&M TOTAL	24.23		21.92	14.45	4.26 - 79.76	8.27	31.36
O&M w/o grinding energy costs *	18.79		16.56	9.92	3.13 - 58.58	6.33	25.07

Tab. J-4: Energy share of reported O&M costs. Data extracted from Table 4 in Daniel, Lane and McLean (22):

	Mine A SABC	Mine A HPGR	Mine B SABC	Mine B HPGR	Mine C SABC	Mine C HPGR	average	stdev
Power cost (\$/t)	1.39	1.18	1.03	0.87	0.78	0.62	0.98	0.28
Operating cost total /\$/t)	2.86	2.2	2.46	1.88	2.17	1.63	2.20	0.43
relative share of power costs (%)	48.6	53.6	41.9	46.3	35.9	38.0	44.06	6.70

Tab. J-5 Summary of costs for mining, crushing, grinding, spreading and distribution. Sources: ^aEnerdata (32); ^bRenforth et al.(41); ^cThrikawala (42), no uncertainty range given, therefore $\pm 25\%$ are assumed here.

Parameter	Unit	Best Estimate	Lower Bound	Upper Bound
Comminution				
Specific investment costs	US \$ t ⁻¹ rock a ⁻¹	5.0	2.8	13.5
Operation and maintenance costs	US \$ t ⁻¹ rock	25.1	9.9	58.6
Electricity demand (50/20/10/2 μm)	GJ t ⁻¹ rock	0.07/0.20/0.46/3.0	0.02/0.07/0.17/1.4	0.24/0.61/1.2/6.1
Electricity price ^a	US \$ GJ ⁻¹	23.8	19.2	32.3
Electricity costs (50/20/10/2 μm)	US \$ t ⁻¹ rock	1.67/4.76/10.9/71.4	0.38/1.34/3.26/26.9	7.75/19.7/38.8/197
Transportation to fields ^b	US \$ t ⁻¹ rock km ⁻¹	0.05	0.05	0.05
Spreading on fields				
Diesel costs ^c	US \$ t ⁻¹ rock	14.2	10.7	17.8
Specific O&M costs ^c	US \$ t ⁻¹ rock	12.1	9.1	15.1
Total costs (50/20/10/2 μm) at 300 km transportation	US \$ t ⁻¹ rock	73.1/76.2/82.3/143	47.9/48.8/53.8/74.4	127.8/139.7/158.8/317

Source reports in order of appearance in Tab. J-1 and Tab. J-2

Dupere, M., Gagne, J., Gagnon, G., & Baril, F. (SGS Canada Inc.).(2013). Preliminary Economic Assessment of Authier Lithium Property, Quebec, Canada, NI-43-101.

Duplessis, C., Cassoff, J., Rivard, S., Bilodeau, M., Buchanan, M., & Skiadas, N. (2013). Technical Report – Phosphate Resource Estimation update 2013 of the Lac a Paul Property Deposit, NI 43-101.

Fisher, A., Moran, A., Spiller, D.; Evans, D., Yang, D., Garcia, D., Rodrigues, F., Daviess, F., Marrou, J., Mountjoy, K., Clarke, P., & Chapel, T. (SRK Consulting). (2013). Prefeasibility Study of the Toroparu Gold Project, Upper Puruni River Area, Guyana, NI 43-101.

Flint, D.C., Kunkel, K., Gorman, M.G., Moore, D.B., & Wilson, S.E. (Allied Nevada Gold Corp. & Scott E. Wilson Consulting, Inc.). (2012). Technical Report Allied Nevada Gold Corp. Hasbrouck Property, Tonopah, Nevada, USA.

Sedore, M., & Masterman, G. (Kinross Gold Corporation). (2012). Tasiast Mine Mauritania 43-101F1 Technical Report.

Board, W., Kennedy, R., & Yeomans, T. (2011). Technical Report on the Pirquitas Mine, Jujuy Province, Argentina, NI 43-101.

Christie, G., Kulla, G., Ulansky, R., Lipiec, T., Healy, P., Levy, M., Borntraeger, B. (2010) Kitsault Molybdenum Project; British Columbia, Canada NI 43-101 Technical Report on Feasibility Study

Huss, C., Snider, J., Marek, J., Parshley, J., & Drielick, T. (2008). Mount Hope Project – Molybdenum Mine and Process Plant Feasibility Study, NI 43-101.

Lane, R., Giroux, G., & Meintjes, T. (2013). Preliminary Economic Assessment for the Deer Horn Gold-Silver-Tellurium Property, NI 43-101.

Lambert, R., Gow, N., Hampton, A., & Gochnour, L. (Roscoe Postle Associates Inc.). (2012). Technical Report on the El Morro Project, Region III, Chile, NI 43-101.

Gray, J., & Robillard, H. (Moose Mountain Technical Services). (2013). Technical Report for the Kwanika Property, Preliminary Economic Assessment, NI 43-101.

Flint, D.C., Gorman, M.G., Harris, D., Moore, D.B., Peterson, A.T., & Wilson, S.E. (Allied Nevada Gold Corp. & Scott E. Wilson Consulting, Inc.). (2012). Technical Report Allied Nevada Gold Corp. Hycroft Mine, Winnemucca, Nevada, USA.

Arseneau, G., Dance, A., Duncan, J., Elliott, C., Liskowich, M., Murphy, B., Mackie, D., Rykaart, M., & Pilotto, D. (SRK Consulting). (2013). Preliminary Economic Assessment for the Springpole Gold Project, Ontario, Canada.

Elfen, S., Davis, B., & Scott, K. (Ausenco). (2013). Taca Taca copper/gold molybdenum project: Preliminary economic assessment.

K. Distance to source distribution, case Indonesia

The smallest ways, which connect roads given in applied the transport way dataset (23) with the application area, are not mapped out entirely. It is thus necessary to create a buffer zone around the mapped pathways to account for missing connections and reach all cropland. Exemplary data for the region of Indonesia (IDN) show that different buffer distances (Fig. K-1), which represent the unmapped smallest roads connecting application areas with larger roads, do not affect the general distribution of source distances. It can thus be assumed that areas that are not reached follow the general pattern of reachability and can therefore be included in the calculation.

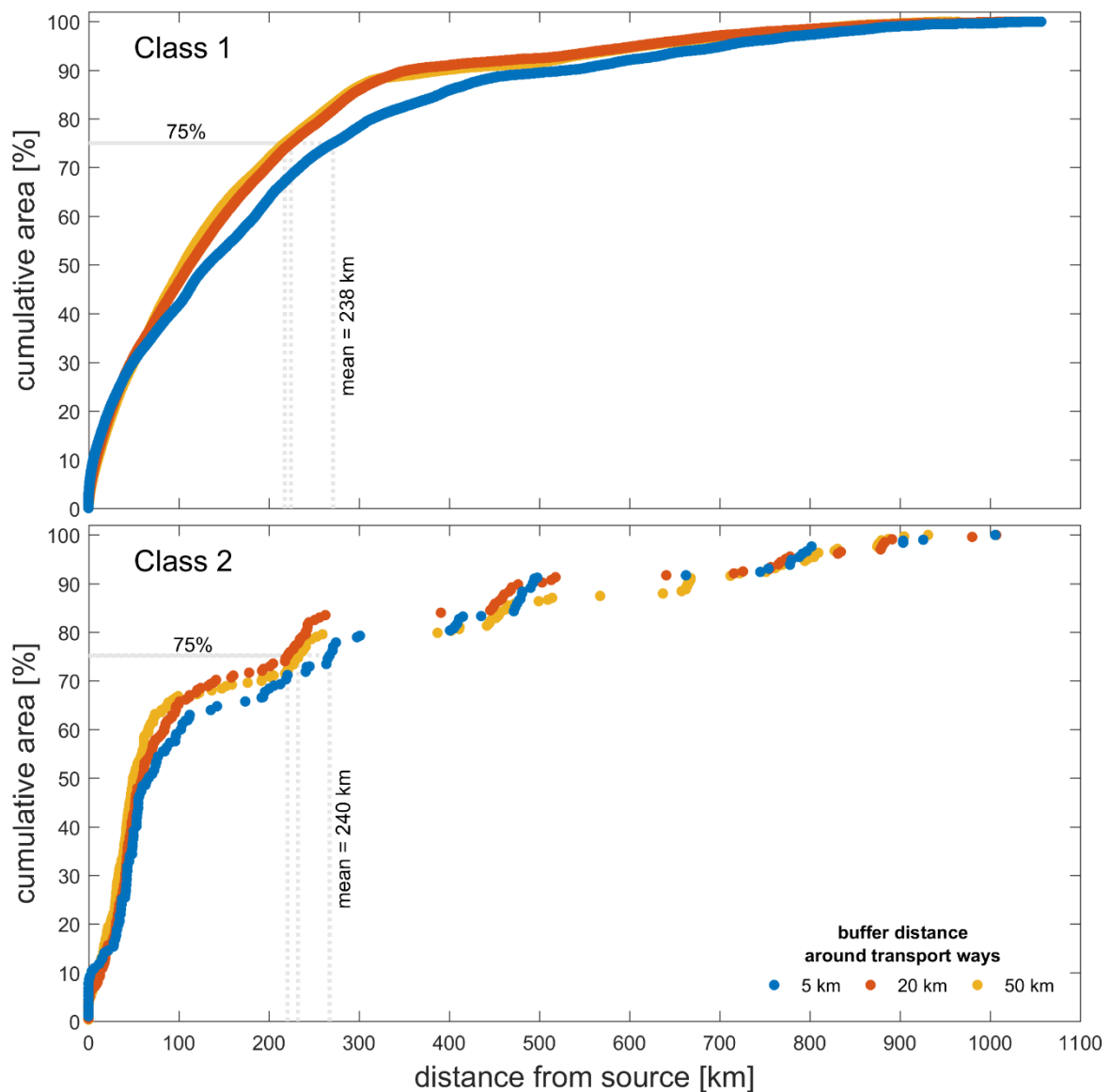


Fig. K-1 Cumulative area based on the distance between source rock and application area in dependence of the buffer distance that is used between transport roads for warm (grade 1) and temperate (grade 2) regions. The relative cumulative area is calculated by summing up the areas starting from the smallest distance from source. 75% of the total area are within a range of about 240 km, considering the average results of 5, 20, and 50 km buffer.

L. Distribution of source rocks

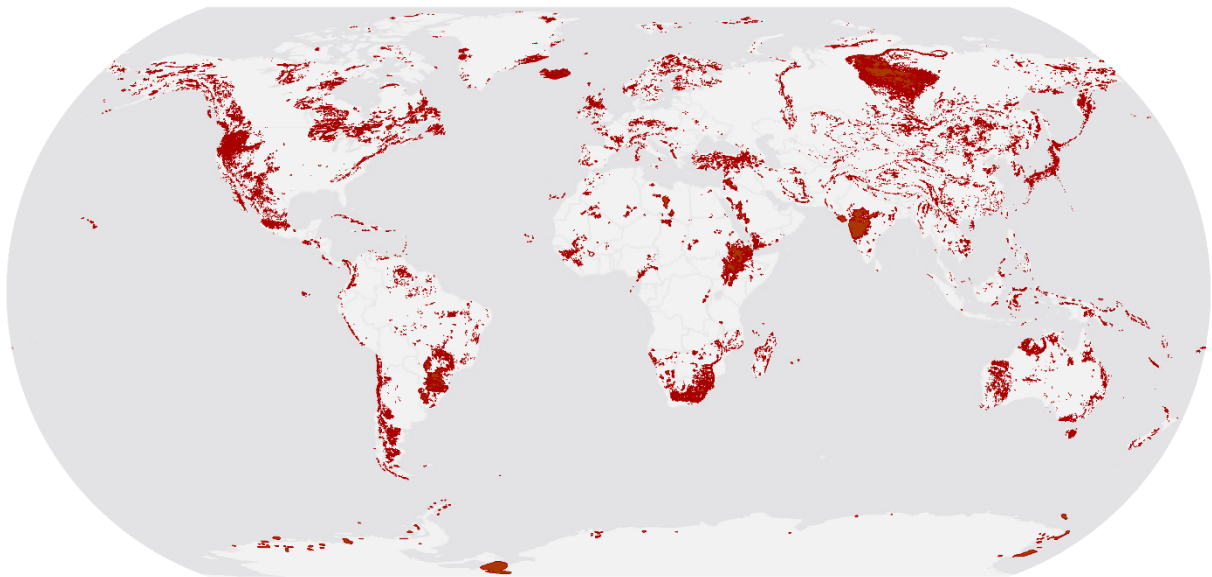


Fig. L-1 Appearance of potential source rocks (red). Data taken from the global lithological map GLiM (24), classes vb and pb, basic volcanics and plutonics respectively. Coverage may appear large than actual observations due to scaling effects for the figure.

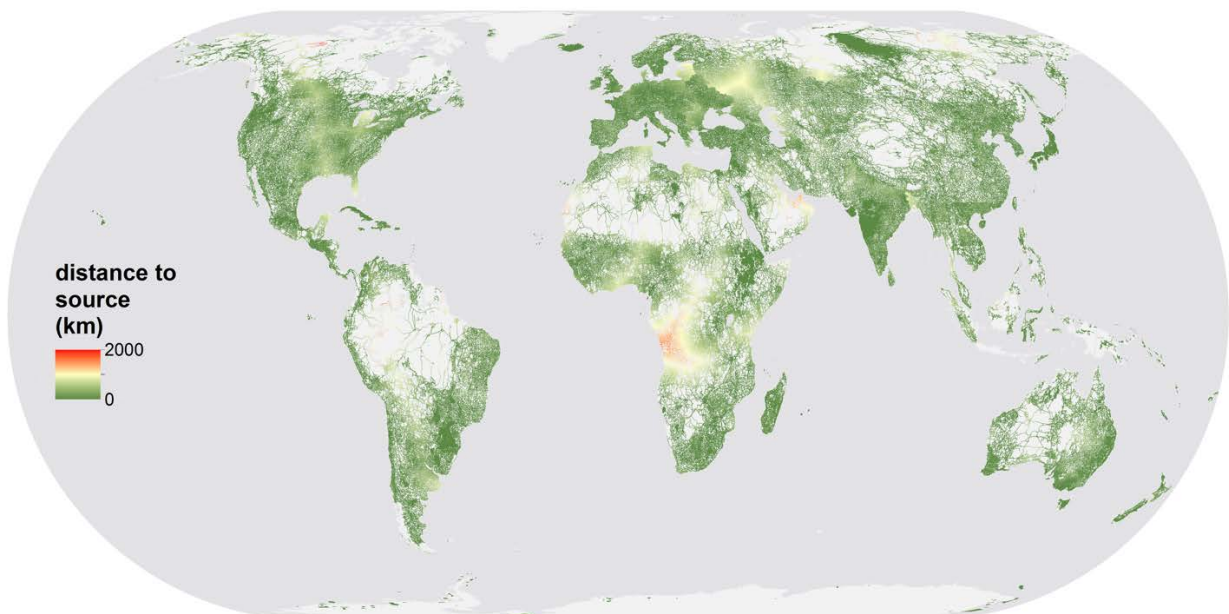
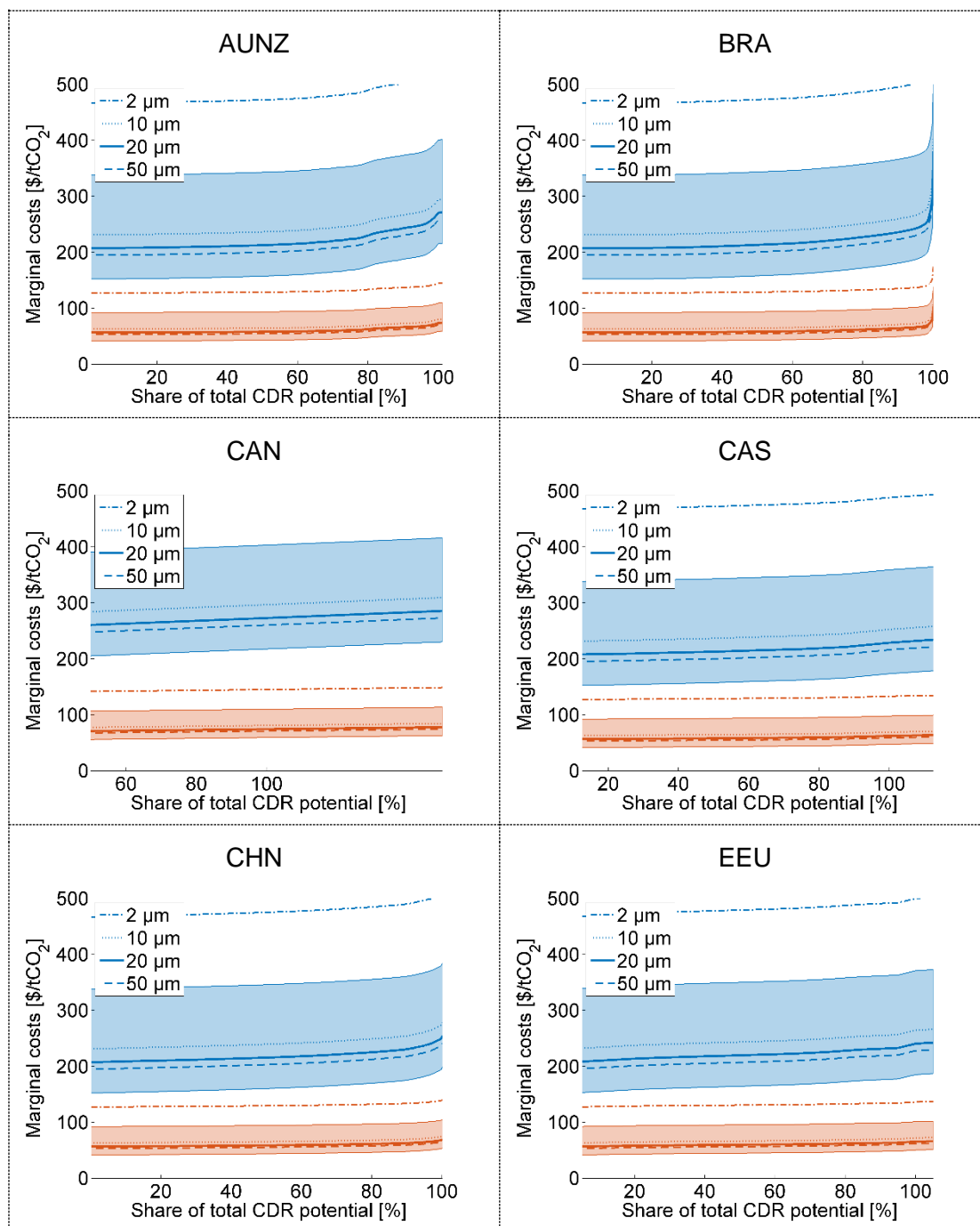


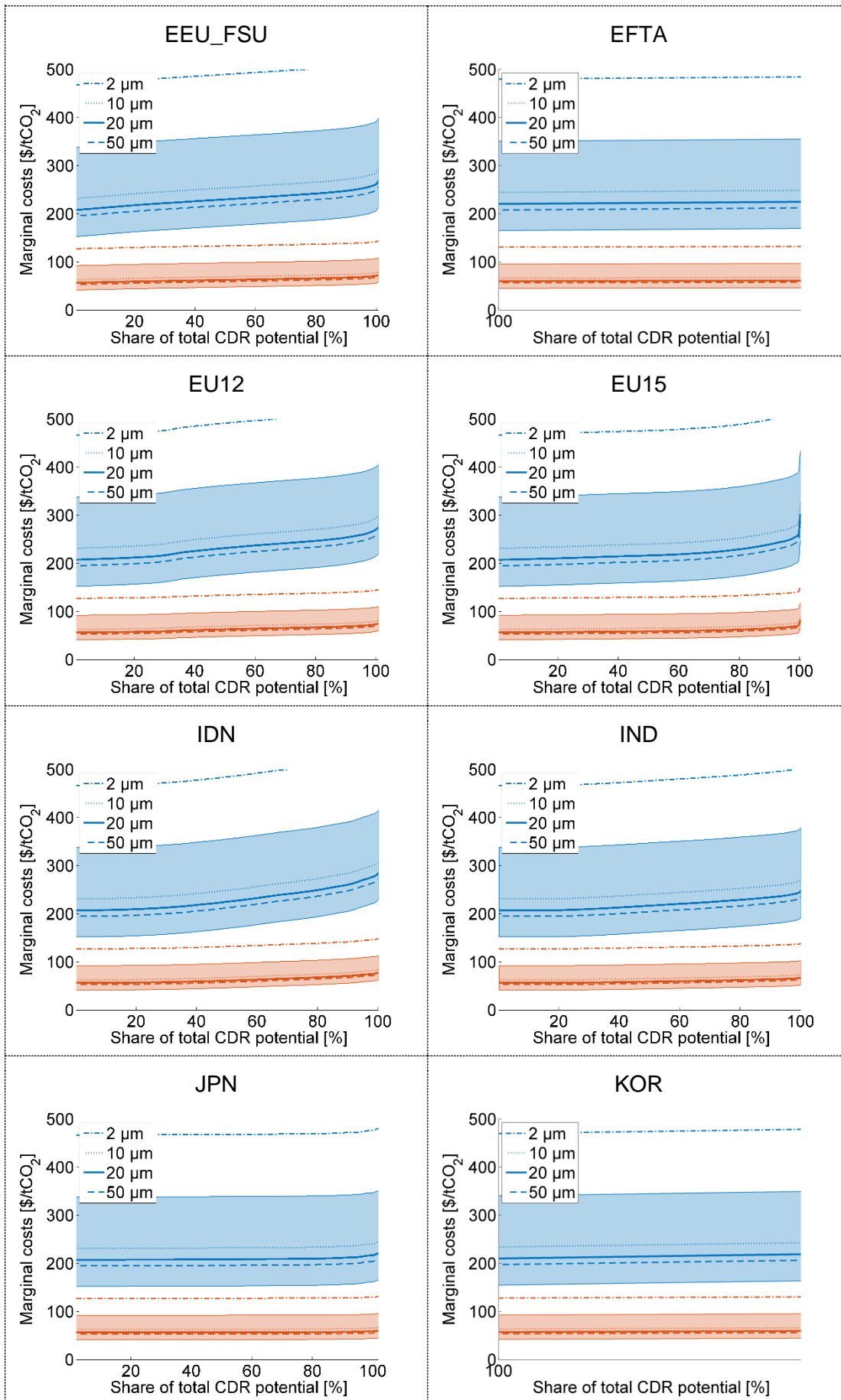
Fig. L-2 Indication of transport distances away from rock sources, based on a cost distance raster data (ArcGIS function), combined from source rock distribution and transport way raster. Resolution: 1km. Please note that sudden color changes can occur at boundaries of economic units as trade across the boundaries was not considered in the model, but may happen in reality.

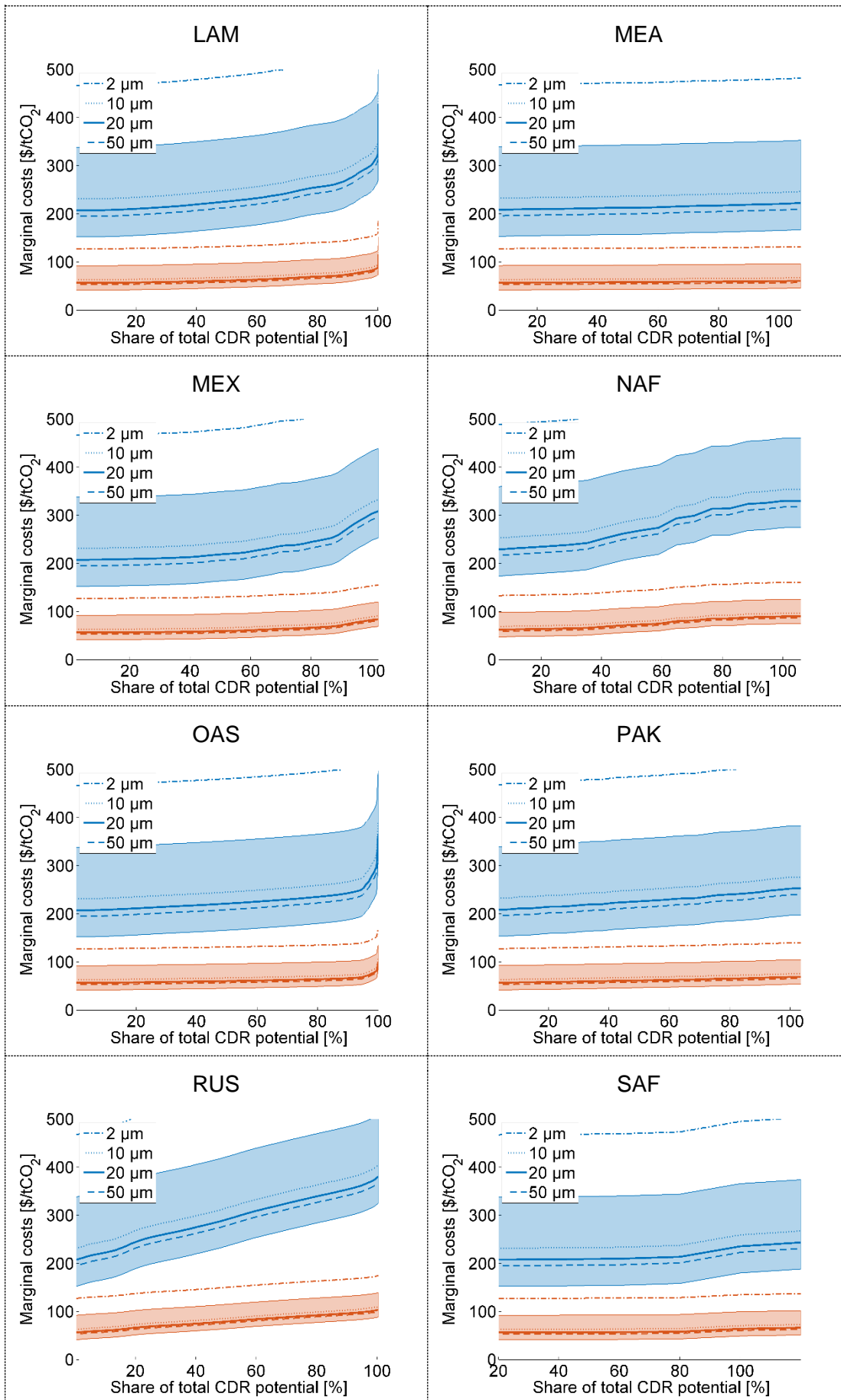
M. Regional supply curves

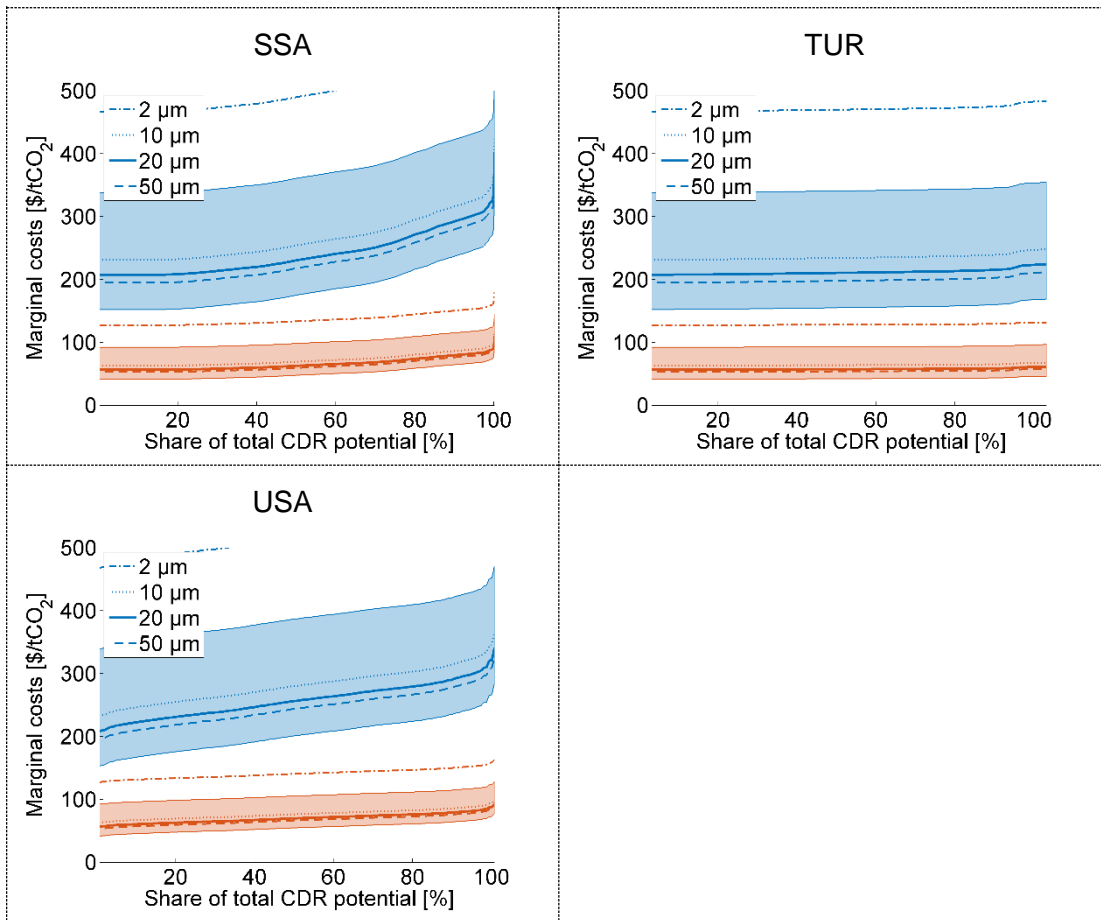
Regional supply curves for carbon removal with EW (see Fig. 5 in the main text) with regional definition according to SI I.

Fig. M-1: Regional supply curve for carbon removal with EW for basalt (blue) and dunite (red) for grain sizes of 2, 10, 20, and 50 μm . The cost uncertainty is shown exemplary for 20 μm .









N. References

1. Köhler P, Hartmann J, & Wolf-Gladrow DA (2010) Geoengineering potential of artificially enhanced silicate weathering of olivine. *P Natl Acad Sci USA* 107(47) :20228-20233.
2. Moosdorf N, Renforth P, & Hartmann J (2014) Carbon dioxide efficiency of terrestrial enhanced weathering. *Environ Sci Technol* 48(9) :4809-4816.
3. Renforth P (2012) The potential of enhanced weathering in the UK. *International Journal of Greenhouse Gas Control* 10(0) :229-243.
4. Sarbas B (2008) The GEOROC Database as Part of a Growing Geoinformatics Network. in *Geoinformatics 2008 –Data to Knowledge*, eds Brady SR, Sinha AK, & Gundersen LC (USGS, Potsdam) , pp 42 - 43.
5. Brantley SL & Mellott NP (2000) Surface area and porosity of primary silicate minerals. *American Mineralogist* 85(11-12) :1767-1783.
6. Chen Y & Brantley SL (2000) Dissolution of forsteritic olivine at 65°C and $2 < \text{pH} < 5$. *Chemical Geology* 165(3– 4) :267-281.
7. Wogelius RA & Walther JV (1991) Olivine dissolution at 25°C: Effects of pH, CO₂, and organic acids. *Geochim. Cosmochim. Acta* 55(4) :943-954.
8. Hangx SJT & Spiers CJ (2009) Coastal spreading of olivine to control atmospheric CO₂ concentrations: A critical analysis of viability. *International Journal of Greenhouse Gas Control* 3(6) :757-767.
9. Renforth P, Pogge von Strandmann PAE, & Henderson GM (2015) The dissolution of olivine added to soil: Implications for enhanced weathering. *Appl Geochem* 61:109-118.
10. Jankovic A, Dundar H, & Mehta R (2010) Relationships between comminution energy and product size for a magnetite ore. *J S Afr I Min Metall* 110(3) :141-146.
11. Bond FC (1961) Crushing & Grinding Calculations: Part II. *British Chemical Engineering* (8) :1.
12. Baláž P, *et al.* (2008) Structural changes in olivine (Mg, Fe) 2SiO_4 mechanically activated in high-energy mills. *International Journal of Mineral Processing* 88(1-2) :1-6.
13. Fabian M, *et al.* (2010) The influence of attrition milling on carbon dioxide sequestration on magnesium– iron silicate. *Minerals Engineering* 23(8) :616-620.
14. Summers CA, Dahlin DC, Rush GE, O'Connor WK, & Gerdemann SJ (2005) Grinding methods to enhance the reactivity of olivine. *Minerals & Metallurgical Processing* 22(3) :140-144.

15. Huijgen WJJ, Ruijg GJ, Comans RNJ, & Witkamp G-J (2006) Energy Consumption and Net CO₂ Sequestration of Aqueous Mineral Carbonation. *Industrial & Engineering Chemistry Research* 45(26) :9184-9194.
16. Hartmann J, Moosdorf N, Lauerwald R, Hinderer M, & West AJ (2014) Global chemical weathering and associated P-release — The role of lithology, temperature and soil properties. *Chemical Geology* 363(0) :145-163.
17. Hijmans RJ, Cameron SE, Parra JL, Jones PG, & Jarvis A (2005) Very high resolution interpolated climate surfaces for global land areas. *International Journal of Climatology* 25(15) :1965-1978.
18. Bandstra JZ & Brantley SL (2008) Data Fitting Techniques with Applications to Mineral Dissolution Kinetics. *Kinetics of Water-Rock Interaction*, eds Brantley SL, Kubicki JD, & White AF (Springer New York) , pp 211-257.
19. Sayre R, *et al.* (2014) A New Map of Global Ecological Land Units—An Ecophysiological Stratification Approach. (Association of American Geographers, Washington, DC) , p 46.
20. Arino O, *et al.* (2008) GlobCover: the most detailed portrait of Earth. in *ESA Bulletin* 136, pp 24-31.
21. Curry JA, Ismay MJL, & Jameson GJ (2014) Mine operating costs and the potential impacts of energy and grinding. *Minerals Engineering* 56(0) :70-80.
22. Daniel M, Lane G, & McLean E (2010) Efficiency, economics, energy and emissions - Emerging criteria for comminution circuit decision making. *XXV International Mineral Processing Congress (IMPC)* , pp 3523-3531.
23. NIMA' (2000) Vector Map Level 0 (VMAP0) . ed Agency NIAm (National Imagery and Mapping Agency, Bethesda, MD) , pp NIMA Reference Numbers VMAP0EURNASIA, VMAP0NOAMER, VMAP0SASAU, VMAP0SOAMAFR.
24. Hartmann J & Moosdorf N (2012) The new global lithological map database GLiM: A representation of rock properties at the Earth surface. *Geochem Geophys Geosy* 13.